scientific reports

Check for updates

OPEN

Mapping NK cell diversity in response to COVID-19 and mRNA vaccination

Yosuke Kishi[1,2], Yu-Chen Liu[1], Masakazu Ishikawa[1], Maika Yamashita[1], Hisatake Matsumoto[3,4], Hiroshi Ogura[3,4], Shuhei Sakakibara[5,6]✉ & Daisuke Okuzaki[1,4,7,8]✉

Human NK cells exhibit functional heterogeneity, yet the clinical conditions and cellular processes driving this diversity remain insufficiently understood. Here, we report that NK cell diversity emerges during peripheral development, influenced by the divergence of adaptive NK cells from various stages of canonical NK cell maturation during the resolution phase of severe COVID-19. Using scRNA-seq, we analyzed blood NK cells from patients with severe COVID-19 (acute phase and post-intensive care), individuals vaccinated with the SARS-CoV-2 mRNA vaccine (BNT162b2), and healthy donors. The frequencies of immature CD56^{bright} and proliferating NK cells increased following BNT162b2 vaccination. In contrast, the frequency of adaptive CD56^{dim} cells was markedly elevated in patients recovering from severe COVID-19, alongside clonal expansion and enhanced mitochondrial oxidative phosphorylation. Trajectory analysis revealed a bifurcation in peripheral NK cell development, with CD56^{bright} cells diverging into canonical and adaptive CD56^{dim} subsets during the course of severe COVID-19. Notably, adaptive NK differentiation exhibited transcriptional and signaling profiles analogous to those of T-cell activation. Thus, NK cell diversity is shaped by the induction of an intrinsic adaptive program. These findings uncover the mechanisms underlying NK cell heterogeneity and have implications for medical applications, including the development of immunotherapies that leverage adaptive NK cell functions.

Keywords NK cells, COVID-19, mRNA vaccine, scRNA-seq, Trajectory analysis

Natural killer (NK) cells are critical components of innate immune effectors and significant contributors to acquired immunity, playing a pivotal role in protective immunity against viral infections and cancer[1]. In humans, NK cells comprise diverse subsets, each performing distinct functions during infection. Conventional flow cytometric analysis categorizes NK cells into two primary subsets based on surface phenotypes. The CD56^{dim} subset, which predominates in peripheral blood, is characterized by its potent natural cytotoxicity. In contrast, the CD56^{bright} subset, which is considered developmentally immature and less cytotoxic, exhibits a high capacity for cytokine production[2,3].

Recent advancements in high-dimensional immune cell characterization have revealed a remarkable diversity of NK cells, highlighting their capacity to differentiate into memory-like adaptive subsets[4–6]. Adaptive NK cells exemplify the versatile functionality of NK cells in innate and adaptive immunity[7,8]. These cells exhibit potent "missing self" reactivity against target cells, rendering them highly effective in combating cancers and infectious diseases[9,10]. Notably, a subset of adaptive NK cells displays antigen presentation potential through the stimulatory expression of human leukocyte antigen (HLA) class II molecules[11]. Adaptive NK responses were shown to be induced by viral antigens derived from human cytomegalovirus (HCMV), or by combined stimulation with IL-12, IL-18 and IL-15[12,13]. Despite well-documented evidence of NK cells adapting to diverse

[1]Laboratory for Human Immunology (Single Cell Genomics), Immunology Frontier Research Center, The University of Osaka, Osaka, Japan. [2]Faculty of Medicine, The University of Osaka, Osaka, Japan. [3]Department of Traumatology and Acute Critical Medicine, Graduate School of Medicine, The University of Osaka, Osaka, Japan. [4]Center for Infectious Disease Education and Research, The University of Osaka, Osaka, Japan. [5]Laboratory of Systems Immunology, Immunology Frontier Research Center, The University of Osaka, Osaka, Japan. [6]Graduate School of Medical Safety Management, Jikei University of Health Care Sciences, Osaka, Japan. [7]Center for Infectious Disease Education and Research, Institute for Open and Transdisciplinary Research Initiatives, The University of Osaka, Osaka, Japan. [8]Japan Agency for Medical Research and Development-Core Research for Evolutional Science and Technology (AMED-CREST), The University of Osaka, Osaka, Japan. ✉email: sakakibara@ifrec.osaka-u.ac.jp; dokuzaki@ifrec.osaka-u.ac.jp

immunological stimuli, the underlying biological processes and cellular mechanisms driving human NK cell diversity remain unclear. This knowledge gap is primarily attributed to the limited studies analyzing clinical samples suitable for assessing NK cell diversification within the periphery.

The emergence of coronavirus disease 2019 (COVID-19), caused by severe acute respiratory syndrome coronavirus 2 (SARS-CoV-2), has highlighted the crucial role of dysregulated immune responses in the development of severe respiratory diseases. Key contributors include the excessive production of pro-inflammatory cytokines, exacerbated T-cell cytotoxicity, and generation of pathogenic autoantibodies[14–16]. Several studies have investigated the role of NK cells in controlling SARS-CoV-2 infection and COVID-19 pathogenesis. A reduction in peripheral blood NK cell numbers, alongside other lymphocyte populations, has been consistently observed during acute COVID-19[17,18]. A longitudinal study identified early IFNα signatures and persistent NK cell dysfunction in patients with severe COVID-19[19]. Additionally, TGFβ response signatures in NK cells have been implicated as a characteristic feature of severe COVID-19, contributing to impaired cytotoxic function[20]. These findings highlight variability in the functional characteristics of NK cells across individual studies in the context of COVID-19.

The widespread deployment of mRNA vaccines has been instrumental in mitigating the COVID-19 pandemic. Emerging evidence indicates that SARS-CoV-2 mRNA vaccination induces both quantitative and qualitative changes in the NK cell compartment. A study revealed that vaccine recipients exhibited a decrease in $CD16^{hi}$ NK cell number and an increase in the proportion of IFNγ-secreting NK cells[21]. Additionally, a high baseline frequency of $NKG2C^{+}$ adaptive NK cells was correlated with enhanced antiviral antibody titers after SARS-CoV-2 mRNA vaccination[22], suggesting the involvement of adaptive NK cells in bridging innate and acquired immune responses. However, the effects of mRNA vaccination on the functional diversification of NK cells to lead enhance antiviral immunological memory remain elusive.

This study aimed to explore the diversification of human NK cells, particularly adaptive NK cell subsets, under varying immunological conditions. Single-cell RNA sequencing (scRNA-seq) serves as a powerful technique for elucidating the heterogeneity and developmental trajectories of immune cells in clinical samples, making it essential for understanding complex biological processes. However, the high cost of scRNA-seq typically constraints experimental designs, limiting the range of conditions and time points that can be examined. To circumvent this limitation, we integrated scRNA-seq data from our cohort with a publicly available dataset to conduct a comparative analysis of NK cell populations in peripheral blood mononuclear cells (PBMCs); the study cohort comprised patients with severe COVID-19 at different time points after disease manifestation, individuals vaccinated with the SARS-CoV-2 mRNA vaccine (BNT162b2), and healthy donors.

Results

Single-cell landscape of blood NK cells from patients with COVID-19, SARS-CoV-2 mRNA-vaccinated individuals, and healthy controls

To compare NK cell diversity under different immunological conditions, we analyzed the single-cell transcriptome of peripheral blood NK cells across different immune states (Fig. 1a). This included publicly available scRNA-seq data of PBMCs from patients with acute severe/critical COVID-19 admitted to the intensive care unit (ICU) (T1, upon ICU admission) and healthy individuals (E-GEAD-551)[23]. These patients received mechanical ventilation, corticosteroids, and anticoagulants during their ICU stay. Additionally, we included data from patients with severe COVID-19 during the resolution phase after treatment in the same hospital (T2, 6–19 days after ICU admission [Table 1]) and healthy individuals who received the BNT162b mRNA vaccine in a two-dose regimen, with samples collected 7–11 days after the second dose (Table 2). We integrated the scRNA-seq data from a total of 34 patients: five healthy controls, seven vaccinated individuals, sixteen patients with severe COVID-19 at T1, and six patients at T2. The donor information is summarized in Supplementary Table S1.

After data integration, cells from each donor group showed a similar distribution in the UMAP plot. (Supplementary Fig. S1a). From the combined PBMC datasets, we selected clusters 2, 7 and 8, which expressed authentic NK markers, *KLRD1*, *KLRF1*, *NKG7*, and *GNLY* (Supplementary Fig. S1b, and c). During data processing, we excluded cells expressing gene markers for T cells (*CD3D* and *CD3G*), B cells (*IGHG1*, *IGHG2*, and *JCHAIN*), macrophages (*LYZ*), platelets (*PPBP*), and erythrocytes (*HBA1*), as detailed in the Methods section (Supplementary Fig. S1d). After data processing, 30,684 NK cells were retained for subsequent analyses. The NK cell cluster definition was validated by the previously used definition of 13 NK cell marker genes previously used[6], supporting their reliability (Supplementary Fig. S1d). The number of NK cells per individual sample is presented in Supplementary Fig. S1e. A k-nearest neighbor (KNN)-based differential abundance analysis using Milo[24] revealed a proportional increase in NK cell number in patients with severe COVID-19 at T2; however, no such alteration was observed in the NK cell populations in patients at T1 or vaccinated donors compared with healthy individuals (Supplementary Fig. S1f).

Using the Leiden algorithm for clustering, nine putative NK clusters were identified in PBMCs from healthy controls, vaccinated donors, and patients with severe COVID-19 at T1 and T2 (Supplementary Fig. S2a). Traditionally, NK cells have been classified into subsets based on surface phenotype[25,26]. However, this approach was not feasible for scRNA-seq analysis owing to the limited presence of cells expressing authentic NK differentiation markers, such as *NCAM1* (CD56), *B3GAT1* (CD57), *CD27*, and/or *ITGAM* (CD11b) (Supplementary Fig. S2b). Instead, these clusters were classified based on their transcriptomic profiles into five functional subsets: $CD56^{bright}$, canonical $CD56^{dim}$, transitional, adaptive $CD56^{dim}$, and proliferating (Fig. 1b, c, and Supplementary Fig. S2c). The $CD56^{bright}$ subset was marked by increased expression of *SELL*, *IL7R*, and *GZMK* and decreased expression of *FCGR3A*, *PRF1*, and *GZMB*, representing the immature NK phenotype, relative to other subsets. In contrast, the canonical $CD56^{dim}$ subset, corresponding to conventional cytotoxic effector NK cells, exhibited the highest levels of *FCGR3A*, *PRF1*, *NKG7* and *CCL4* expression among NK subsets. Moreover, another subset expressing these effector genes, but at intermediate levels, was identified;

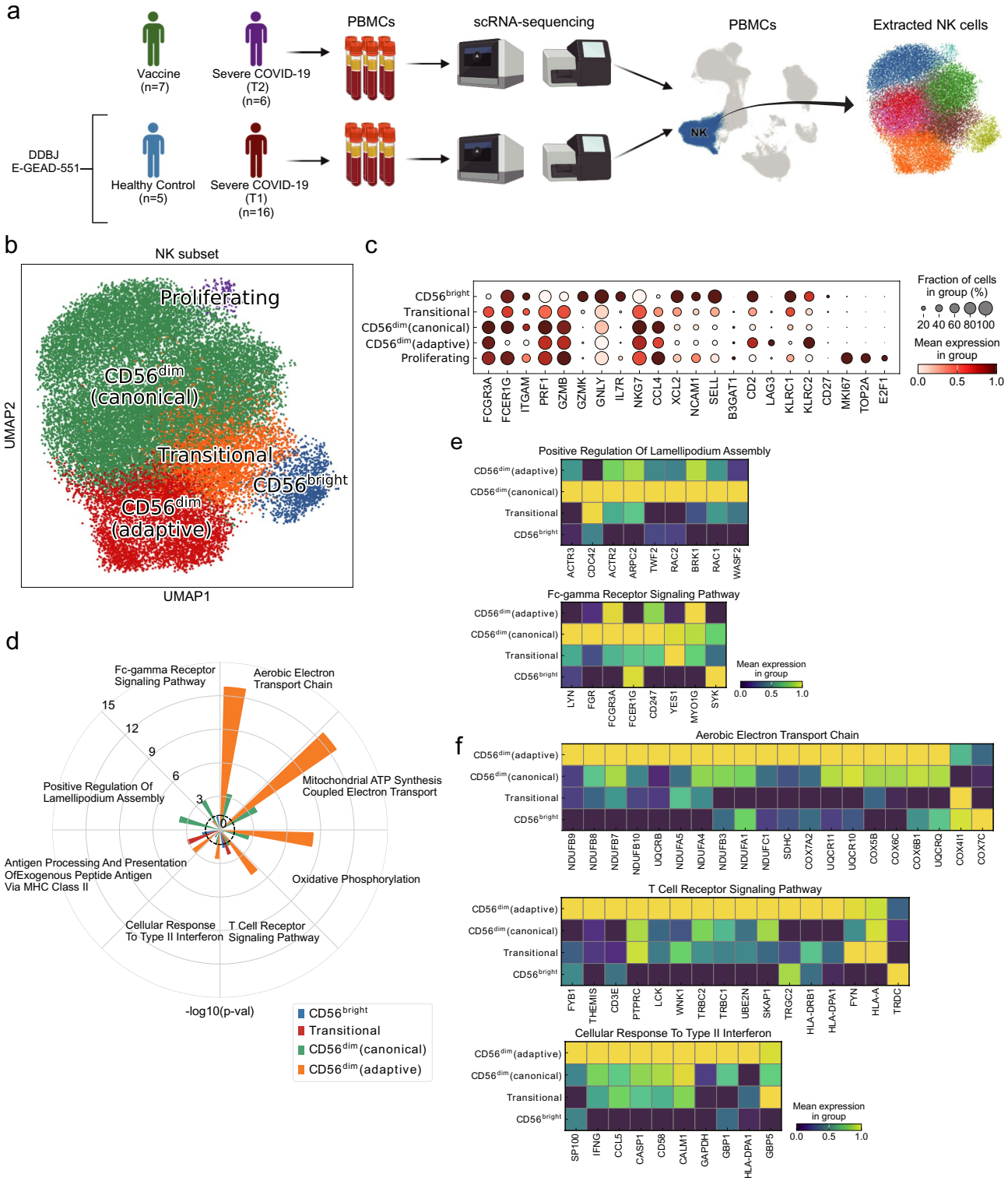

Fig. 1. Single-cell RNA sequencing (scRNA-seq) analysis for mapping human NK cell subsets in peripheral blood. (**a**) Schematic illustrating the workflow for data collection and analysis of human natural killer (NK) cells under various immunological stimuli using scRNA-seq. (**b**) Uniform manifold approximation and projection (UMAP) embedding of scRNA-seq data for 30,684 NK cells. Cells are color-coded by NK cell subsets: CD56^{dim}, canonical (green), CD56^{dim}, adaptive (orange), CD56^{dim}, transitional (red), CD56^{bright} (blue), and proliferating (purple). (**c**) Dot plots showing the expression of selected marker genes across five NK subsets. (**d**) Selected Gene Ontology (GO) biological process terms enriched in the NK cell subsets, excluding proliferating NK cells. The combined score represents – log10(p-value) * z-score. (**e, f**) Matrix plots showing the expression of genes in the selected GO biological process terms, highlighting genes upregulated in CD56^{dim} (canonical) (**e**) and CD56^{dim} (adaptive) NK cells (**f**).

Patient ID	Age (y)	Sex	Blood collection (days at ICU)	BMI	PaO2 (mmHg)	FiO2 (mmHg)	P/F ratio	SARS-COV-2 infection status at blood collection (antigen test)			HCMV infection status
								Nasopharyngeal swab	Sputum	Blood	
T2_01	62	M	8	25.9	148	1	148	+ve	+ve	−ve	+ve
T2_02	60	F	10	19.6	82.5	0.9	91.7	+ve	+ve	ND	+ve
T2_03	62	M	9	ND	68.4	0.7	91.7	+ve	ND	ND	+ve
T2_04	79	F	10	25.7	137	1	137	ND	ND	ND	+ve
T2_05	67	M	9	33.2	104	1	104	ND	ND	ND	ND
T2_06	74	M	8	22.3	83.7	0.6	139.5	+ve	ND	+ve	+ve

Table 1. Demographic data of patients. ND: not determined.

Donor ID	Age (y)	Sex	Days after 2nd vaccination	HCMV infection status
VP_01	44	F	9	+ve
VP_02	36	F	8	+ve
VP_03	25	M	7	-ve
VP_04	37	F	9	+ve
VP_05	32	F	7	+ve
VP_06	24	F	11	+ve
VP_07	24	F	7	+ve

Table 2. Demographic data of vaccinated donors.

this subset was designated as transitional NK cells. The adaptive CD56^{dim} NK cell subset was characterized by high expression of *KLRC2* and low levels of *KLRC1*, *FCER1G*, and *ITGAM* (CD11b) when compared with that of other subsets (Fig. 1c). This classification of adaptive CD56^{dim} NK cells was further validated through gene signature analysis using a previously established adaptive NK signature[4] (Supplementary Fig. S2d). Finally, the proliferating NK cell subset consisted of cells with elevated expression of cell cycle marker genes such as *Mki67*, *TOP2A*, and *E2F1*. All differentially expressed genes (DEGs) for each subset are shown in Supplementary Fig. S3a. Enriched biological processes in each subset, compared to the others, are shown in Supplementary Fig. S3b. Notably, our analysis revealed the presence of a diverse range of human NK cell subsets in the blood, which were delineated by integrating data from various immunological conditions.

Pathway enrichment analysis of DEGs revealed enhanced cellular motility ("Positive regulation of lamellipodium assembly") as well as Fc receptor signaling ("Fc-gamma receptor signaling pathway") in the canonical CD56^{dim} NK cell subset, compared with that in other subsets (Fig. 1d, e). In contrast, the adaptive CD56^{dim} subset exhibited enrichment in pathways related to T cell receptor signaling ("T cell receptor signaling pathway"), immune response ("Cellular response to type II interferon", and "Antigen processing and presentation of exogenous peptide antigen via MHC class II"), as well as upregulated mitochondrial functions, ("Aerobic electron transport chain", "Mitochondrial ATP synthesis coupled electron transport", and "Oxidative phosphorylation") (Fig. 1d, f). TCR signaling pathway was found to be markedly enriched in the adaptive NK subset, as indicated by increased expression of signal mediators and related molecules, including *CD3E*, *PTPRC*, *LCK*, and *FYN*, which are common signaling adaptors and regulators shared between T and NK cells[27–29]. These findings suggest that canonical NK cells were primarily involved in enhanced motility and effector functions relative to other subsets, whereas adaptive NK cells acquired antigen presentation capabilities and displayed marked alterations in cellular signaling and metabolic pathways.

Distinct NK cell subset compositions elicited by different immunological stimuli and temporal profiles: increased adaptive CD56^{dim} frequency in patients with COVID-19 at T2 and CD56^{bright} after vaccination

We next characterized condition-specific NK cell responses by analyzing changes in subset composition and pathway enrichment. Supplementary Fig. S4 presents the proportions of NK cell subsets across individual samples and donor groups.

In vaccinated individuals, differential abundance analysis revealed an increase in the frequency of proliferating NK cells and a reduction in transitional NK cell levels compared to healthy donors (Fig. 2a). Additionally, certain neighborhoods within the CD56^{bright} subset were enriched in the vaccinated cohort (Fig. 2a). Gene set enrichment analysis (GSEA) revealed the upregulation of various pathways in CD56^{bright} NK cells post-vaccination, compared to those in other subsets. These included "Positive regulation of nucleic acid-templated transcription", "Regulation of the cell cycle", "Negative regulation of nucleic acid-templated transcription", "Regulation of RNA metabolic processes", and "Chromatin remodeling" (Fig. 2b). These findings suggest that the mRNA vaccine may affect NK cell maturation and functionality.

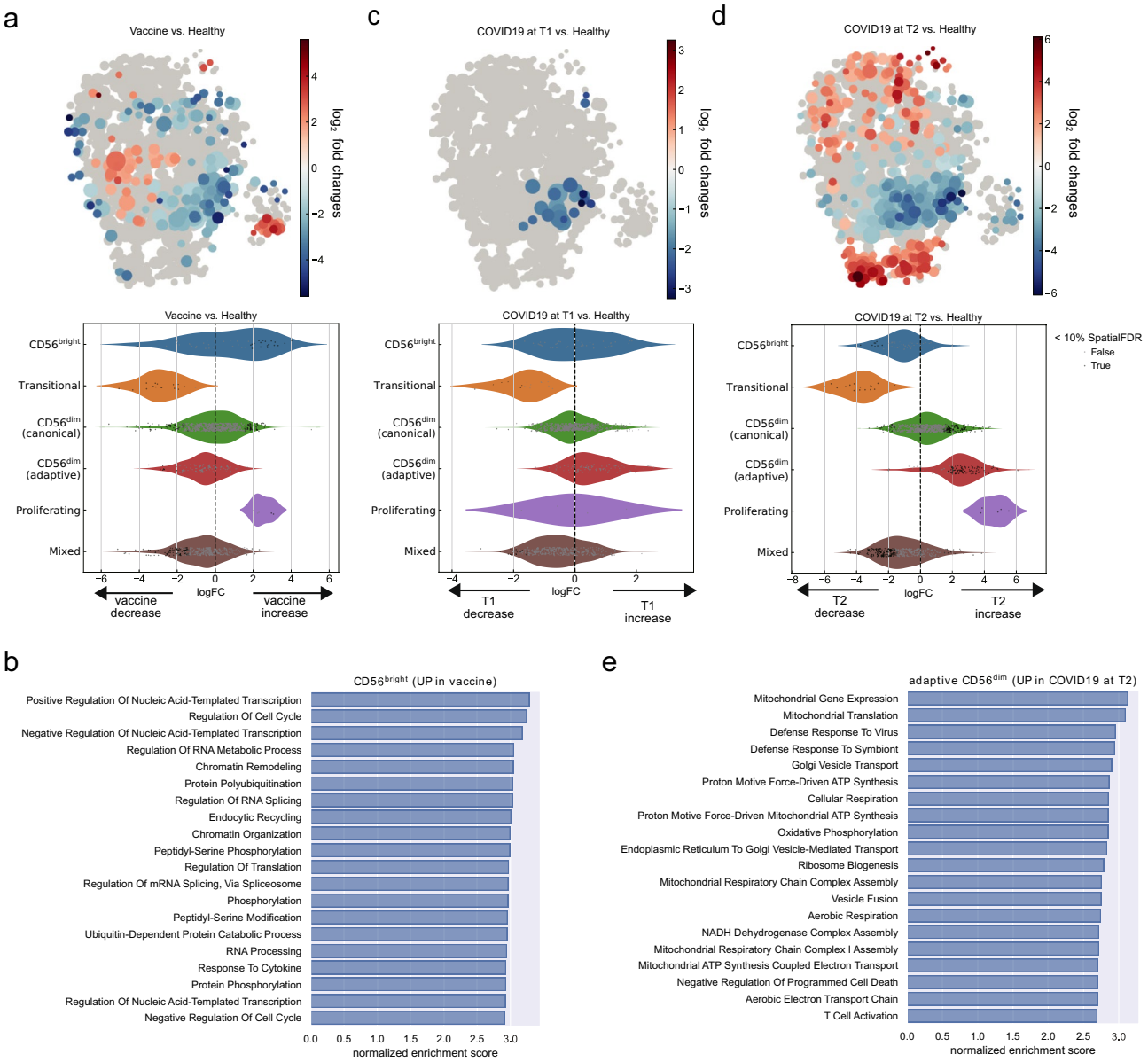

Fig. 2. Distinct NK cell subset compositions elicited by different immunological stimuli and temporal profiles. (**a**) Differential abundance analysis comparing NK cells between vaccinated individuals and healthy controls. Top: Neighborhood graph on UMAP embedding. Each dot represents a neighborhood identified by Milo and is colored according to the log-fold change from the differential abundance test. Bottom: Beeswarm plots showing the distribution of log-fold changes across annotated neighborhoods. Each dot represents a neighborhood and is color-coded to indicate whether the false discovery rate (FDR) is ≤ 0.10. (**b**) Gene set enrichment analysis (GSEA) of the CD56^{bright} subset from vaccinated individuals. (**c, d**) Differential abundance analysis for NK cells from patients with coronavirus disease 2019 (COVID-19) at T1 (**c**) and T2 (**d**) compared with healthy controls. (**e**) GSEA of the adaptive CD56^{dim} subset from patients with severe COVID-19 at T2.

In contrast, the NK cell subset composition was comparable between healthy donors and patients with severe COVID-19 at T1, except for a slight reduction in transitional NK cell levels in patients with severe COVID-19 (Fig. 2c). However, NK cells from patients with COVID-19 at T2 were characterized by an increase in the levels of adaptive CD56^{dim} and proliferating NK subsets, alongside a decrease in the frequency of transitional and CD56^{bright} NK subsets (Fig. 2d). GSEA suggested that adaptive CD56^{dim} NK cells in patients with severe COVID-19 at T2 exhibited increased mitochondrial activity and enhanced oxidative phosphorylation compared with those in other subsets (Fig. 2e).

Direct comparison of abundance and gene enrichment between T1 and T2 are shown in Supplementary Fig. S5. These analyses highlighted increased frequencies of adaptive CD56^{dim} and proliferating NK cell subsets, as well as enhanced mitochondrial functions across all NK subsets in patients with severe COVID-19 at T2

compared to T1. These results highlight the dynamic changes in NK cell responses during the progression of severe COVID-19.

Clonal selection and expansion signatures in adaptive NK cells from patients with severe COVID-19 during the resolution phase

Clonal selection followed by expansion is a key characteristic of adaptive immune responses following antigen-specific stimuli, a phenomenon now extended to innate lymphocytes, as recent studies have suggested that they also undergo clonal expansion during infection[30]. Unlike T and B cells, which generate unique antigen receptors through genetic rearrangement, NK cells express a repertoire of germline-encoded receptors. Therefore, conventional methods for determining clonal relatedness of NK cells based solely on receptor expression are limited, given the potential plasticity of NK cells[31].

To examine whether the NK cell response following vaccination and during COVID-19 is driven by clonal expansion, we leveraged the inferred heteroplasmy of mitochondrial single-nucleotide variations (SNVs) in scRNA-seq data. In total, 34 informative mitochondrial SNVs were identified from patients with COVID-19 at T2 and vaccinated donors using MQuad[32]. The patterns of mitochondrial SNVs and their mutation frequencies, estimated via mRNA analysis, were used to determine clonal structures (Supplementary Fig. S6a), identifying 26 clones (Supplementary Table S2). Examination of the homogeneity within the single-cell transcriptomes of these clonal NK cells revealed five clones (T2_02_6249G>A, T2_02_6285G>A, T2_02_15084G>A, T2_04_1945A>C, and T2_04_2838A>G), derived from two patients, with each exhibiting a connectivity score > 1.5 and demonstrating significant transcriptional correlation (false discovery rate [FDR] < 0.05) (Fig. 3a).

Notably, these clones were exclusively detected within the adaptive CD56^{dim} NK cell subset of the corresponding donors (Fig. 3b–d), indicating a homogeneous expansion of NK cells within this subset. Although not restricted, these donors, T2_02, and T2_04, possessed HCMV-specific IgG, suggesting persistent HCMV infection (Table 1). Furthermore, these clones exhibited distinct expression patterns of NK receptors (Fig. 3b, c), suggesting clonal selection driven by specific target recognition. Several other clones, such as T2_01_7657T>C and T2_05_1729T>C, identified in patients with COVID-19 at T2 were relatively small and predominantly distributed across subclusters within the canonical CD56^{dim} and transitional NK cell subsets (Supplementary Fig. S6b). In contrast, no clones with significant transcriptional homogeneity (FDR < 0.5) were detected in vaccinated donors.

Some identified clones, including VP_07_24442T>C spanned across the CD56^{bright}, transitional, and canonical CD56^{dim} subsets but not within the adaptive CD56^{dim} subset (Supplementary Fig. S6b). These results highlighted the homogeneity of adaptive NK cell clones, in contrast to the intraclonal diversity observed across transitional and canonical CD56^{dim} NK cells, during COVID-19 treatment, as observed previously in HCMV-positive healthy donors[5].

Bifurcated developmental trajectory of NK cells during the resolution of COVID-19

To investigate the developmental trajectory of adaptive CD56^{dim} NK cells in our dataset, we employed scFates, a tool designed for pseudotime analysis that infers developmental bifurcations from single-cell transcriptomic data[33]. Given the observed increase in the frequency of adaptive CD56^{dim} NK cells in patients with severe COVID-19 during disease resolution, compared to that in other conditions (Fig. 2c, d), we focused on the single-cell transcriptomes of NK cells from these patients.

Using combined data from patients with COVID-19 at T1 and T2, we constructed a multi-scale diffusion space using Palantir, which generated a principal tree graph that identified a bifurcated developmental trajectory for NK cells, with node 155 from the CD56^{bright} subset serving as the root (Fig. 4a). The trajectory segments and milestones defined by the principal tree graph corresponded well with the NK cell subsets identified in the single-cell transcriptome, except the "transitional" milestone, which comprised a large proportion of the canonical CD56^{dim} subset, alongside small fractions of transitional and adaptive CD56^{dim} cells (Fig. 4b). The bifurcation began at the transitional NK milestone, leading to the emergence of adaptive and canonical CD56^{dim} subsets (Fig. 4c). Cell density changes along pseudotime indicated that the divergence toward adaptive CD56^{dim} NK cells was initiated at T1, followed by further adaptive maturation at T2, whereas divergence toward canonical CD56^{dim} NK cells was observed at both time points (Fig. 4d). Therefore, the developmental bifurcation from CD56^{bright} to both canonical and adaptive CD56^{dim} NK cells contributed to the observed NK cell diversity in patients with COVID-19.

By extracting DEGs along pseudotime, we identified 366 and 131 genes specific to the developmental trajectories of canonical and adaptive CD56^{dim} NK cells, respectively (Fig. 4e, f, and Supplementary Table S3). Genes associated with the development toward canonical CD56^{dim} NK cells included the authentic markers for canonical NK cells, such as *KLRC1* and *FCGR3A*, as well as cytotoxic effector genes, including *FGFBP2*, *GZMB*, and *PRF1*, along with transcription factors (TFs), such as *TBX21* and *ZBTB16* (Fig. 4e). Conversely, genes that exhibited elevated expression in the adaptive CD56^{dim} NK lineage, relative to the canonical lineage, included *KLRC2*, *CD2*, *CD3E*, as well as HLA class II genes, including *HLA-DP*, *HLA-DQ*, and *HLA-DR* (Fig. 4f). This analysis identified several key regulators involved in NK cell fate determination. Notably, *FCER1G*, a critical receptor component for the maturation of canonical CD56^{dim} NK cells[34], showed increased expression along the developmental trajectory of canonical NK cells (segment 2, Supplementary Fig. S7a); however, its expression drastically decreased during the development of adaptive NK cells (segment 1, Supplementary Fig. S7a). Additionally, several genes were consistently expressed during the development of canonical NK cells; however, their expression decreased in the adaptive pathway. These genes included *ZBTB16* and *TBX21*, essential TFs for the development of innate lymphocytes, including NK cells[35,36], and *THEMIS2*, a critical regulator of NK memory function, as demonstrated in a recent murine study[37] (Supplementary Fig. S7a). The expression of *PTGDS*, previously demonstrated to be expressed in a subset of CD56^{dim} NK cells[38], was strongly induced along

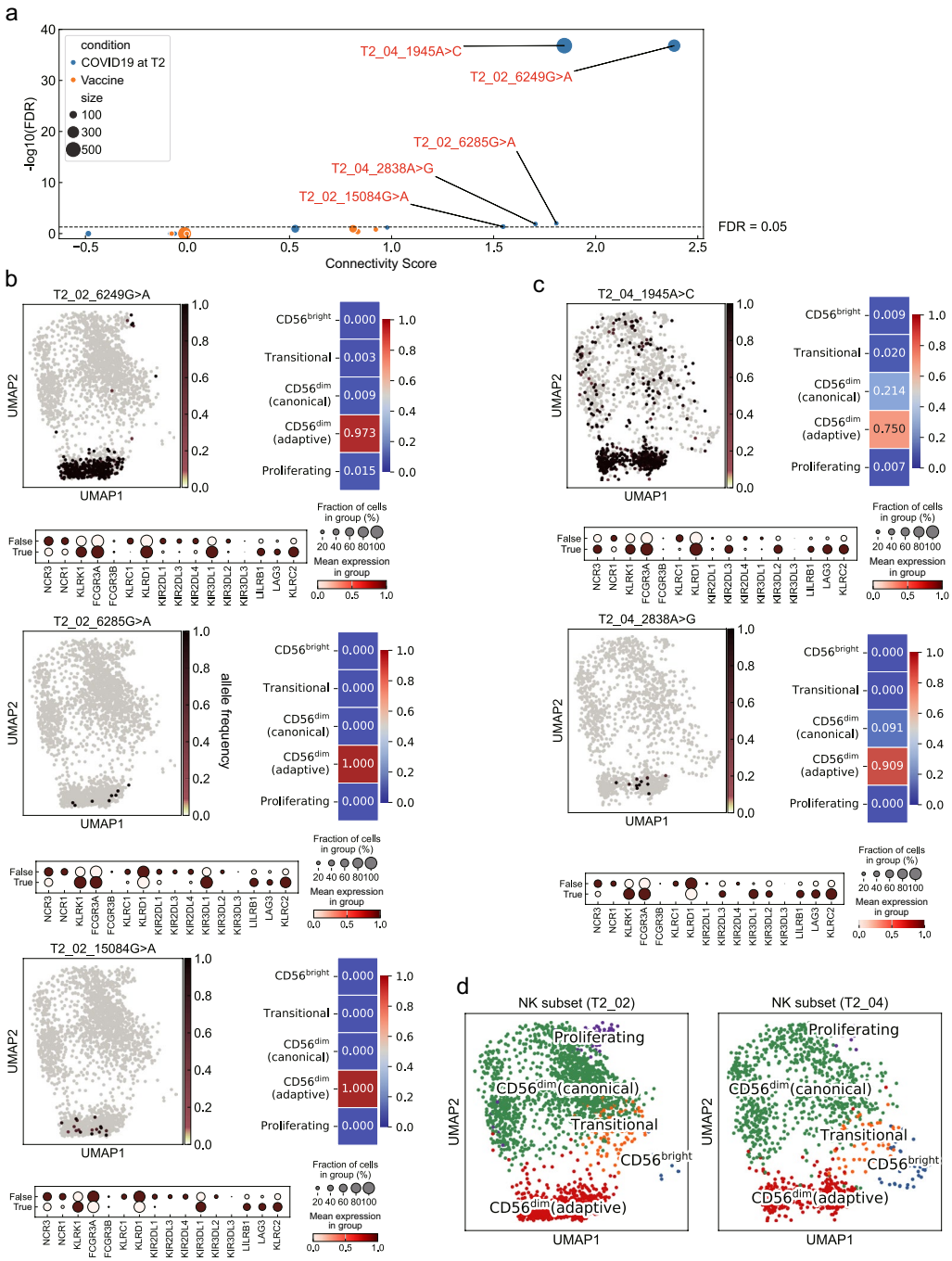

Fig. 3. Clonal expansion of adaptive NK cells in patients with severe COVID-19 at T2. (**a**) Scatter plot of connectivity scores versus log10 (FDR). Each dot represents a clone identified based on informative mitochondrial single-nucleotide variants (SNVs), color-coded by the donor group. Dot size corresponds to the number of cells in each clone. (**b, c**) Top left: UMAP embedding showing the differential abundance of NK cells across each condition, with cells colored according to the allele frequency of mitochondrial SNVs. Top right: Heatmap illustrating the distribution of cells among NK subsets with mitochondrial SNV allele frequency greater than 50%. Bottom: Dot plots showing the expression of NK receptor genes in cells from each clone and the remaining cells from the same donors. (**d**) UMAP embedding of total NK cells from donors T2_02 and T2_04.

the trajectory of canonical NK cells (Supplementary Fig. S7a). These results highlight the accuracy and reliability of this trajectory analysis. Pathway enrichment analysis further revealed a functional enhancement in Fc receptor-mediated processes and cellular motility driven by the cellular cytoskeleton. Notable pathways included "FCGR3A-related phagocytosis", "RHO GTPases activate WASPs and WAVEs", and "EPHB-mediated forward

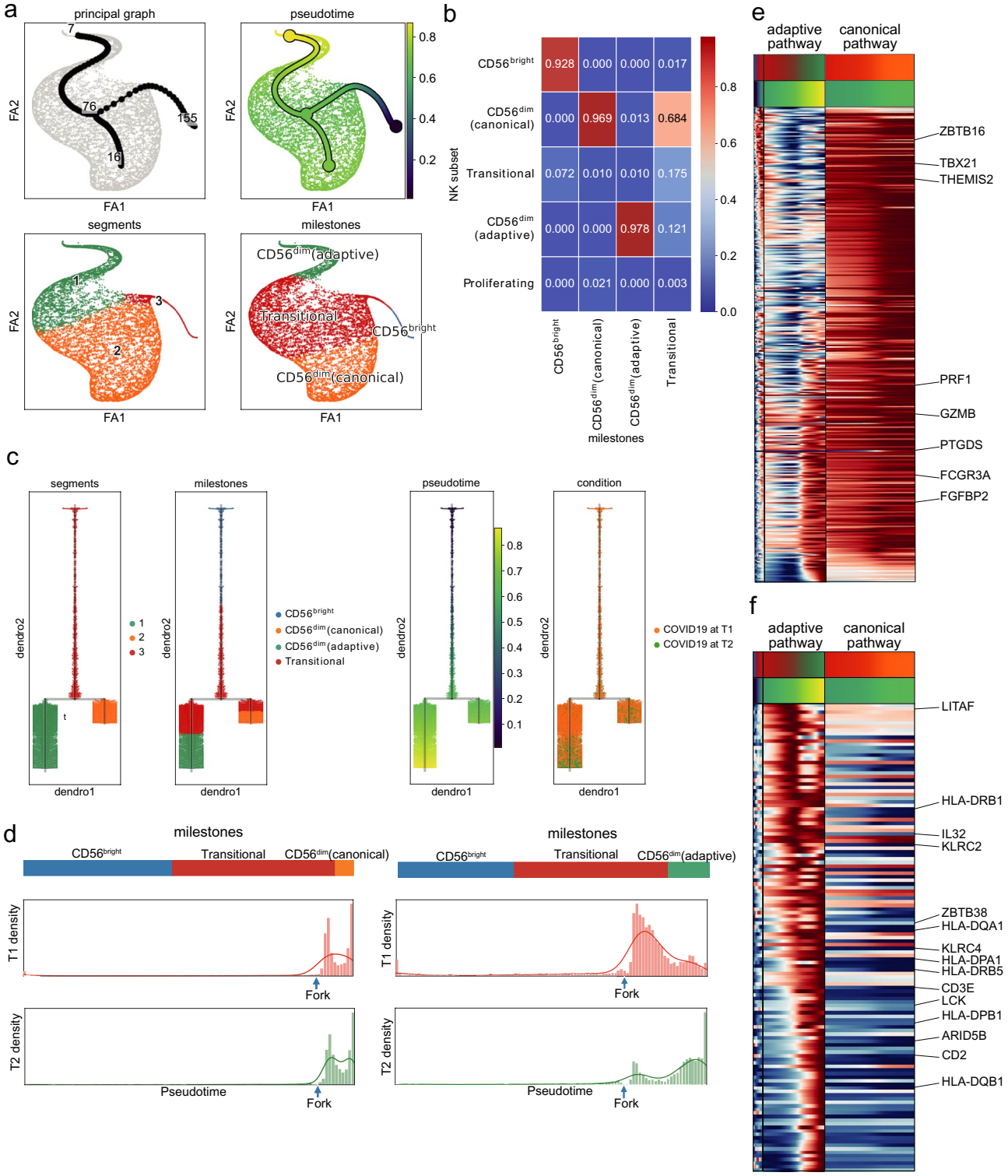

Fig. 4. Bifurcated developmental trajectory of NK cells in patients with severe COVID-19 at T2. (**a**) ForceAtlas2 graph embedding multi-scale diffusion spaces. Top left: Principal graph generated using SimplePPT. Each number represents a root, fork, or end node. Top right: Pseudotime assignment for each cell, determined based on the principal graph after root selection. Bottom: Cells annotated by segments (bottom left) and milestones (bottom right). (**b**) Heatmap showing NK cell subset distribution across milestones. Column sum to 1. (**c**) Dendrograms of NK cell distribution by segment, milestone, pseudotime, and condition. (**d**) Density plots illustrating NK cell distribution over pseudotime. Left: Canonical NK developmental pathway. Right: Adaptive NK developmental pathway. (**e, f**) Scaled expression of differentially expressed genes (DEGs) along pseudotime in the canonical (**e**) and adaptive (**f**) NK developmental branches. Featured gene names are indicated.

signaling", all of which were enriched in the developmental pathways of canonical NK cells (Supplementary Fig. S7b).

In the adaptive NK cell trajectory, the expression of *KLRC2*, a phenotypic marker for adaptive NK cells, was readily induced (Supplementary Fig. S7c). Additionally, the levels of *ARID5B*, a key TF that promotes mitochondrial membrane potential[39], were increased in the adaptive NK cell trajectory (Supplementary Fig. S7c), consistent with the observed enhancement of oxidative phosphorylation in adaptive NK cells (Fig. 1d). Furthermore, several novel genes associated with adaptive NK cell development were identified, including *IL32*, which encodes a human-specific inflammatory cytokine; *KLRC4*, which encodes NKG2F, an orphan activated receptor on human NK cells[40]; and *ZBTB38* and *LITAF*, TFs with unknown functions in NK cells (Supplementary Fig. S7c). Pathways enriched during adaptive NK cell development included acquired immunity-related signaling pathways and protein translation pathways, such as "Translocation of ZAP70 to the immunological synapse", "Phosphorylation of CD3 and TCR zeta chains", "PD1 signaling", "Generation of second messenger molecules", and "Eukaryotic translation elongation" (Supplementary Fig. S7d). Collectively, our findings highlight the dynamic reprogramming of signal transduction and metabolic regulation throughout the progression of adaptive NK cells.

Gene regulatory networks governing NK cell diversity

Based on transcriptional profiles, we identified the upstream transcriptional regulators involved in the differentiation and function of adaptive and canonical NK cell subsets in patients with severe COVID-19. To extract the TFs governing adaptive and canonical CD56^{dim} NK cell dynamics, we inferred TF activity using the decoupleR package[41], integrating data from time points T1 and T2. For the canonical subset, key TFs predicted to be central to the transcriptional regulatory network included NCOA3, EOMES, MEF2C, MITF, and FOXF2 (Fig. 5a and Supplementary Fig. S8a). Although the identification of NCOA3 is not particularly informative, as it primarily functions as a coactivator for DNA-binding TFs[42], our analysis identified EOMES and MEF2C as important TFs for canonical NK cells. Recent studies have demonstrated that these factors play crucial roles in NK cell development and function in humans[43,44]. Additionally, MITF and FOXF2 are critical for cell differentiation of other cell lineages[45,46], suggesting potential roles for these factors in the functional capacities of canonical NK cells. These findings highlight the need for further investigation into their contributions to NK cell biology.

In adaptive NK cells, several HLA-II enhanceosome factors, including RFXAP, RFXANK, RFX5, and CIITA[47], were identified as highly active TFs (Fig. 5a), indicating a specific upregulation of the expression of HLA-II genes in this subset. This expression profile suggests the potential role of adaptive NK cells in bridging innate and acquired immune responses. Additionally, gene network analysis further identified several key TFs, including NOTO, IRF6, and EHF, which reportedly influence the developmental fate of non-immune cell types[48–50], as being active in adaptive NK cells (Fig. 5a). The gene regulatory network model for adaptive NK cells is shown in Fig. 5b.

When integrated with the developmental trajectories, the scores of the identified regulons were strongly correlated with the individual NK cell developmental pathways (Supplementary Fig. S8b). Notably, the functions of EOMES and MEF2C were suppressed, whereas those of RFXAP and NOTO were enhanced along the development of adaptive NK cells. Overall, these results highlight the presence of distinct transcriptional programs that drive the bifurcation of NK cell development, providing insights into the transcriptional regulation underlying NK cell diversity in peripheral immune responses.

Discussion

Although NK cells are innate lymphocytes with functional heterogeneity[1], the mechanisms underlying the establishment of NK cell diversity remain unclear. In this study, we investigated the functional diversity and developmental trajectories of human NK cells. Using integrated scRNA-seq data from blood NK cells under different immunological stimuli, we observed a notable increase in the number of adaptive NK cells, particularly in patients with severe COVID-19 undergoing ICU treatment. In contrast, patients with acute severe COVID-19 at ICU admission showed no substantial changes in NK cell subset composition compared to healthy controls. This observation is consistent with several previous reports, although some studies have highlighted increased NK cell activation in the blood of patients with COVID-19[51–53]. Despite expansion of CD56^{bright} and proliferating subsets, adaptive NK cells did not increase in proportion within 7–11 days after vaccination; however, longitudinal analysis may yield different results. Trajectory analysis suggests that the formation of adaptive NK cells can be initiated during peripheral NK cell maturation and progresses through a transitional subset between the immature CD56^{bright} to CD56^{dim} subsets (Supplementary Fig. S9). This finding contrasts with the previously proposed linear model of adaptive NK cell development[54].

Furthermore, our findings revealed that adaptive NK cells underwent transcriptional reprogramming involving signaling adaptors, metabolic regulators, and epigenetic regulators during their bifurcation from canonical NK cell development. The adaptive NK cell developmental trajectory in peripheral blood was associated with biological processes related to T-cell activation. Among these, enhancement of PD-1 signaling was also observed in the adaptive NK cell development; nonetheless, its functional relevance remains controversial, given the low or undetectable surface expression of PD-1 on NK cells[55–57]. Cells in the adaptive NK fate also exhibited decreased expression of canonical NK marker genes and regulators, including *FCER1G, TBX21* and *ZBTB16*[58–60], while concurrently exhibiting increased expression of a distinct set of genes, such as *KLRC2* and *ARID5B*. Notably, the levels of *ARID5B*, a pivotal regulator of mitochondrial metabolism in adaptive NK cells[39], were increased during this developmental process. Beyond these developmental associations, our analysis showed upregulation of the FcγR signaling pathway in adaptive NK cells. This may contribute to antibody-dependent

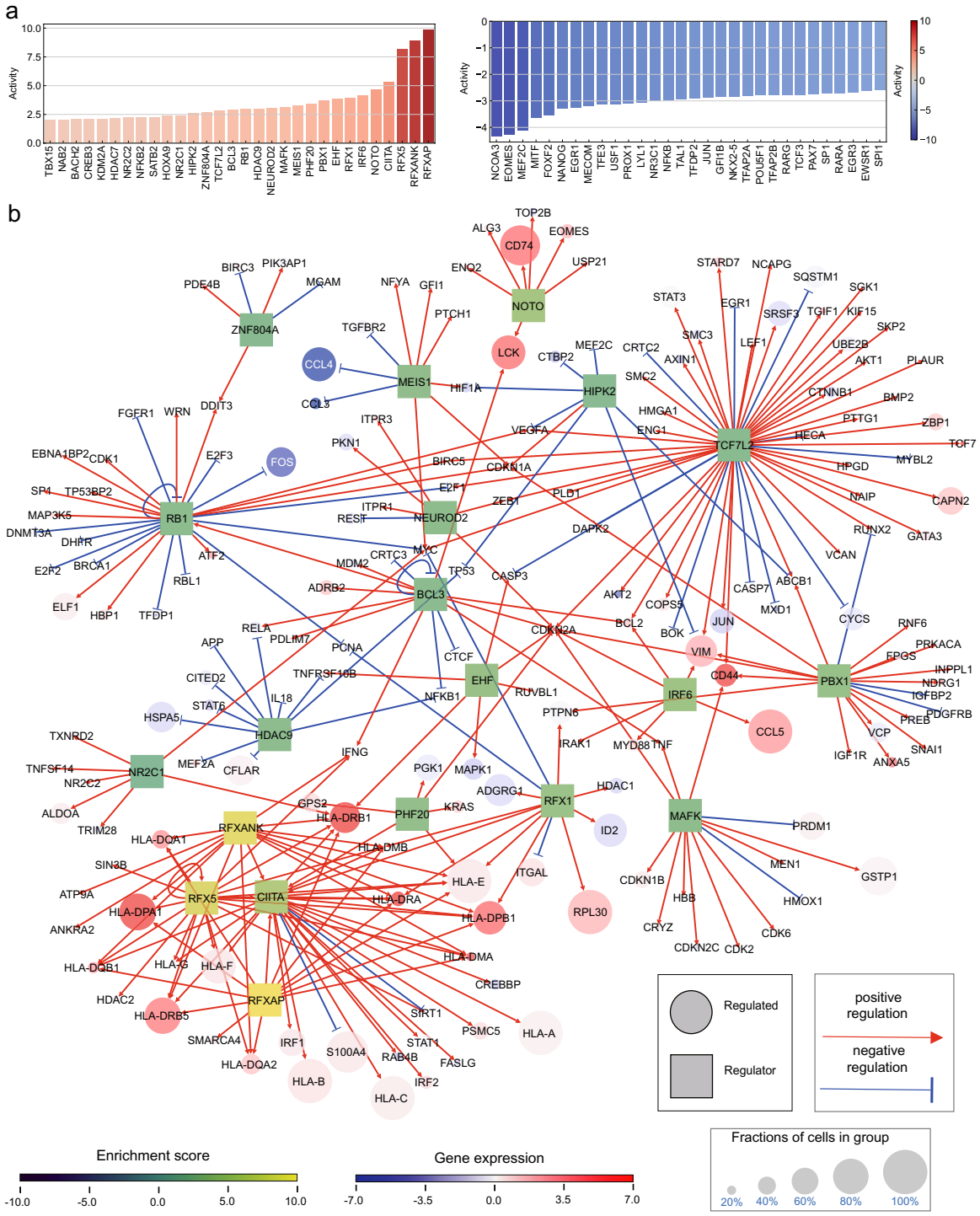

Fig. 5. Prediction of transcriptional regulators governing adaptive NK cell development. (**a**) Bar plots showing the top 30 transcriptional factors (TFs) based on TF activity enrichment scores for canonical and adaptive CD56^{dim} NK cells. Bars are color-coded to reflect the corresponding enrichment scores. (**b**) Gene regulatory network graph of adaptive CD56^{dim} NK cells. Square nodes represent TFs color-coded according to their TF activity enrichment scores. Round nodes represent target genes from CollecTRI color-coded based on their gene expression levels, with size proportional to the fraction of cells in the adaptive CD56^{dim} subset. Red lines indicate positive regulation, whereas blue lines represent negative regulation.

cellular cytotoxicity (ADCC) and facilitate the clearance of virally infected cells through collaboration with the antibody response in these patients.

Additionally, *ZBTB38*, a TF known to bind to CpG-methylated DNA[61], was identified to be associated with the adaptive trajectory-associated transcription, suggesting its potential role in the epigenetic regulation of NK

cell adaptive reprogramming. Chromatin accessibility changes reportedly regulated increased *KLRC2*, *ARID5B* and *ZBTB38* expression as well as reduced *FCER1G and ZBTB16* expression in adaptive NK cells of HCMV-positive donors, whereas these epigenetic changes were not observed in those of HCMV-negative donors[5]. This raises a new question concerning the mechanism by which an HCMV antigen triggers chromatin remodeling that leads to transcriptional reprograming in the adaptive NK cell fate, warranting further investigation in future studies.

Assessment of mitochondrial SNVs revealed several expanded clones within the adaptive CD56^{dim} subset of patients with severe COVID-19 during the resolution phase. Although clone identification was constrained by the high number of cells in the dataset, the methodology employed for clonality assessment proved robust, allowing for effective clonal analysis based on scRNA-seq data. Previous research has demonstrated that ex vivo expansion of NK cells results in plasticity in killer immunoglobulin receptor expression[31,62]. However, our analysis demonstrated that individual clones exhibited distinct expression patterns of NK cell receptors within the adaptive NK compartment of individual donors. This observation suggests that adaptive NK cells undergo clonal selection based on specific target antigens. Consistent with our findings, clonal expansion has also been exclusively observed in adaptive NK cells from the blood of healthy individuals infected with HCMV[5]. Therefore, clonal selection followed by homogenous expansion represents a fundamental aspect of adaptive NK cell formation rather than a feature unique to NK responses in COVID-19. Due to the limited detection of NK cell clones in the dataset, we could not conclude whether clonal proliferation is more enhanced during SARS-CoV-2 infection than after vaccination.

Although our analysis suggests that NK cell divergence is characterized by the expansion of adaptive NK cells in patients with severe COVID-19, the factors driving this process remain unclear. One potential trigger for adaptive NK cell expansion in these patients could be HCMV-derived peptides, as previously demonstrated[5]. Several studies have shown that HCMV was reactivated during severe COVID-19[63,64]. Alternatively, SARS-CoV-2-derived peptides may induce adaptive NK cells. The nonstructural protein 13 (Nsp13) in SARS-CoV-2 contains a peptide ($Nsp13_{232-240}$) that can be presented by HLA-E, preventing its binding to the inhibitory NK receptor NKG2A, thereby inducing a "missing self" activation of NK cells[65]. However, the Nsp13 peptide has been demonstrated to activate NK cells without promoting adaptive NK cell development and expansion in vitro[65]. A recent study has suggested that the YLQPRTFLL peptide from the SARS-CoV-2 spike (S) protein can activate adaptive NK cells and inhibit NKG2A^{+} canonical NK cells[66]. Nonetheless, our analysis of NK cells following mRNA vaccination did not reveal an enhanced adaptive NK response, although the vaccine BNT162b2 encodes SARS-CoV-2 S, which contains the YLQPRTFLL peptide. Therefore, the precise mechanisms responsible for inducing adaptive NK cell expansion in patients with COVID-19 remain elusive.

The BNT162b2 mRNA vaccine elicited an increase in the frequency of CD56^{bright} NK and proliferating cells. These CD56^{bright} NK cells showed distinctive transcriptional signatures and RNA metabolism compared with those of healthy individuals, indicating intrinsic changes in NK cells following mRNA vaccination. This observation aligns with that of previous reports suggesting that the inflammatory phenotypes of NK cells mediate the adverse effects and reactogenicity associated with BNT162b2 mRNA vaccination[67,68]. Although based on limited examples, clonal analysis revealed transcriptional diversification within NK cell clones across the CD56^{bright}, transitional, and canonical CD56^{dim} subsets in vaccinated individuals. This observation likely reflects the rapid clonal development of canonical NK cells, but not adaptive NK cells, in response to vaccination. The absence of adaptive NK cell expansion after vaccination could be attributed to the timing of sample collection. A longitudinal analysis of NK cell subsets after mRNA vaccination will further clarify their persistence and functional changes over time. Alternatively, adaptive NK cells may migrate to tissues after vaccination and contribute to durable protection, as previously shown for T cells[69]; however, whether this also applies to NK cells remains unclear. In this context, evaluating tissue-resident NK cells may provide more insight into adaptive NK cell clonal expansion than analysis of circulating NK cells.

A notable limitation of this study is its relatively small sample size. The conclusions drawn from this study could be strengthened by incorporating additional data into the analysis. Potential confounding factors, including HLA haplotypes, disease history, and HCMV reactivation status, were not addressed. The observed imbalance in age and sex was partly attributed to the higher prevalence of severe COVID-19 in older male patients during the early stages of the pandemic[70]. Clinical treatment during ICU stay may affect NK cell responses, potentially leading to decreased frequencies of conventional CD56^{dim} NK cells in severe COVID-19 patients compared to other groups. Glucocorticoids have been shown to reduce NK cell responsiveness by altering receptor expression[71,72]. Mechanical ventilation increases pro-inflammatory cytokines[73], which may promote memory-like, adaptive NK cell function[12,73]. Lastly, although our conclusions are based on integrated scRNA-seq analysis, experimental validation is required to further elucidate the roles of the identified biological processes in NK cell diversification.

In conclusion, our study revealed that the activation of the intrinsic adaptive program in human NK cells results in their functional diversity in the periphery. Adaptive NK cells diverged from a peripheral transitional subset, and this differentiation was particularly enhanced during the resolution phase of severe COVID-19. This developmental bifurcation was driven by the adaptive reprogramming of NK cells, involving alterations in cellular signaling and metabolism that resemble T-cell activation. Further exploration into the generation of adaptive NK cells may offer valuable insights into immune responses following viral infections and vaccinations. Recent advancements in cellular immunotherapy have proposed the use of NK cells carrying chimeric antibody receptors (CARs) for cancer treatment[74], and in light of the COVID-19 pandemic, several studies have suggested the potential benefits of using CAR NK cells in treating COVID-19[75,76]. Our findings not only provide crucial insights into the functional diversification of human NK cells but also offer valuable guidance for optimizing NK cell-based immunotherapies.

Methods

Clinical samples

Clinical samples were collected with approval from the Osaka University Research Ethics Committee. Written informed consent was obtained from all participants or their relatives before sample collection. Samples were collected from patients with severe COVID-19 (WHO score 5–7) admitted to the ICU at Osaka University Hospital (Osaka, Japan) between November 2020 and December 2021, as well as from healthy individuals vaccinated with the Pfizer-BioNTech SARS-CoV-2 mRNA vaccine (BNT162b2). For patients with COVID-19, infection with the SARS-CoV-2 Alpha.V2 variant was confirmed via PCR at ICU admission. SARS-CoV-2 infection status was intermittently monitored by viral antigen testing in nasopharyngeal swab, sputum and blood during ICU stays. Blood samples were collected upon ICU discharge; four patients were still positive for SARS-CoV-2 antigen and the rest were not tested at that time. These patients received mechanical ventilation, corticosteroids, and anticoagulant medicines during their stay in the ICU. For vaccinated individuals, BNT162b2 vaccine was administered intramuscularly in a two-dose regimen, with doses given a 21-days interval between doses. Blood samples were obtained 10–14 days after the second dose. PBMCs were isolated from blood samples using Lymphoprep (STEMCELL Technologies, Vancouver, BC, Canada) and cryopreserved in the vapor phase of liquid nitrogen according to the manufacturer's protocol.

HCMV serostatus

Persistent HCMV infection in donors was determined by detecting antiviral IgG in plasma using a commercially available kit (Human Anti-Cytomegalovirus IgG ELISA Kit [Abcam]), following the manufacturer's protocol. Samples with OD450 values > 10% exceeding the cut-off control were defined as positive.

scRNA-seq for PBMCs from patients with COVID-19 and vaccinated donors

Frozen PBMCs were thawed at 37 °C and subjected to droplet-based scRNA-seq using Chromium Single Cell V(D)J Reagent Kits v1.1 (10 × Genomics, Pleasanton, CA, USA), following the manufacturer's instructions. Sequencing of the generated cDNA library was performed on an Illumina NovaSeq 6000 platform (San Diego, CA, USA).

scRNA-seq data collection and processing

Previously published scRNA-seq data from patients with COVID-19 and healthy individuals were obtained from the Human Database (hum0366.v1, E-GEAD-551) provided by the National Bioscience Database Center, Japan. The cohort was collected from the same hospital during a similar time period (between December 2019 and October 2021), and had comparable characteristics in terms of age, sex, and disease scores (WHO score 5–7) to those in our ICU COVID-19 cohort[23]. Preprocessed count matrices, which had undergone quality control, were used for further analyses. The collected FASTQ files were processed using Cell Ranger (v5.0.1) with the GRCh38 human reference genome[77].

Quality control, normalization, batch correction, and dimensionality reduction in scRNA-seq analysis

The gene expression matrices filtered by Cell Ranger were analyzed using the Scanpy package (v1.10.3)[78]. We applied the same quality control method to our cohort as used for the public dataset to enable integration[23]. Cells expressing fewer than 100 genes and genes detected in fewer than three cells were excluded. Additionally, cells with fewer than 1,000 unique molecular identifiers (UMIs) or more than 20,000 UMIs, as well as those with over 10% of reads derived from mitochondrial or hemoglobin genes, were excluded. For each sample, doublets predicted using Scrublet (v0.2.3)[79] were removed. Count matrices were normalized using counts per million mapped reads and log-transformed with a log plus one (log1p) transformation. In total, 2,000 shared highly variable genes (HVGs) were identified using the pp.highly_variable_genes() function with flavor = "seurat." Principal component analysis (PCA) was subsequently performed. Batch correction was applied using harmonypy (v0.0.10), a Python wrapper for the Harmony R package[80]. Subsequently, a neighborhood graph was constructed based on the batch-corrected representation, and dimensionality reduction was achieved via uniform manifold approximation and projection[81].

Identification of NK cells in the scRNA-seq dataset

NK cell populations were identified as previously described[82], with slight modifications. Briefly, cells were clustered in an unsupervised manner using the Leiden algorithm[83] with a resolution parameter set to 1.0. Clusters exhibiting NK cell signatures were determined by the expression of classical NK marker genes, *KLRD1*, *KLRF1*, *NKF7*, and *GNLY* as mentioned in previous reports[82]. Subsequently, cells expressing marker genes associated with other lineages, such as *CD3D* and *CD3G* for T cells, *IGHG1*, *IGHG2*, and *JCHAIN* for B cells, *LYZ* for macrophages, *PPBP* for platelets, and *HBA1* for erythrocytes, were excluded. The remaining cells were designated as NK cells in the datasets.

Adaptive NK gene signature scoring

Subclustering of the NK cell subset was performed using the Leiden algorithm. To identify the adaptive NK cell subset, previously described adaptive NK signatures[4] were utilized as input for the scanpy.tl.score_genes() function, replicating the approach implemented in Seurat[84]. Gene scores were calculated by subtracting the average expression of a reference gene set from that of the target gene set. The reference set was randomly sampled from the gene pool for each binned expression value.

Differential cell abundance analysis

Differential cell abundance between conditions (healthy vs. vaccinated, healthy vs. severe T1, and healthy vs. severe T2) was assessed using Milo[24], as implemented in pertpy (v0.9.4)[85]. A KNN graph was constructed with k = 30 based on similarities in the reduced principal component space following batch correction. Neighborhoods were defined based on their connectivity within the KNN graph and subsequently assigned to cells. Counts for each neighborhood were modeled using a negative binomial generalized linear model, and p-values were calculated using the quasi-likelihood F-test under a specified contrast. Spatial FDR correction was applied to control for multiple testing, with a significance threshold set at 10% FDR. Neighborhoods in which cells in a specific annotated subset accounted for less than 75% of the total cell population were designated as "Mixed."

Enrichment analysis of DEGs

To ensure robust analysis, proliferating cells and specific genes— such as ribosomal genes, as well as *TRAV*, *TRAJ*, *TRBJ*, *TRBV*, *IGHV*, *IGKV*, and *IGLV*—were excluded. Differential gene expression analysis was performed using the scanpy.tl.rank_genes_groups() function, which employs the Wilcoxon rank-sum test with p-value correction via the Benjamini–Hochberg method. DEGs were considered statistically significant if they met an adjusted p-value threshold of < 0.05. Functional analysis of DEGs was performed using Gene Ontology (GO) enrichment analysis with the gsea.enrichr() function in GSEApy[86], a Python wrapper for Enrichr[87–89], with GO biological process 2023 or Reactome 2022 as the reference set. GSEA was performed using the gsea.gsea() function, with GO biological process 2023 as the reference set.

Detection of mitochondrial mutations

Mitochondrial SNVs were extracted from raw BAM files for each sample from patients with COVID-19 at T2 and vaccinated individuals using the cellsnp-lite (v1.2.3) tool[90]. Informative mitochondrial SNVs were identified using MQuad (v0.1.8)[32], applying a minimum depth threshold of 5 and a delta Bayesian Information Criterion cutoff of 200. For each informative SNV, allele depth (AD) and depth of coverage (DP) were extracted. Allele frequency (AF) was calculated using the following formula:

$$AF = \frac{AD}{DP + 0.0001}$$

Clones were defined as sets of SNVs with an AF threshold exceeding 0.5. To identify transcriptionally associated SNVs, a connectivity score for each SNV was computed using the scirpy.tl.clonotype_modularity() function in the Scirpy package[91]. The connectivity score was calculated using the following formula:

$$\text{Connectivity score} = \log_2 \frac{|E|_{\text{actual}} + 1}{|E|_{\text{expected}} + 1}$$

where $|E|_{\text{actual}}$ represents the number of edges connecting cells within a given clonotype, and $|E|_{\text{expected}}$ denotes the number of edges that would be expected by random chance in a subgraph of the same size. For each unique SNV size, the expected number of edges was derived by randomly sampling 1,000 subgraphs from the transcriptomic neighborhood graph. A negative binomial distribution was fitted to the background distribution of these edges, and connectivity scores were calculated accordingly. Subsequently, p-values were adjusted for multiple testing using the Benjamini–Hochberg FDR correction method.

Pseudotime analysis

Pseudotime analysis was performed using the scFates tree analysis pipeline (v1.0.8)[33]. During the preprocessing stage, 1,500 HVGs of NK cells were identified from patients with severe COVID-19 at both T1 and T2. PCA was performed, followed by batch correction using harmonypy. Diffusion maps were generated from the batch-corrected representation, and the multi-scale diffusion space was constructed using the first three eigenvectors, as determined by Palantir (v1.3.3)[92]. From the multi-scale diffusion space, a ForceAtlas2[93] embedding was generated using the first two principal components as the initial positions, employing the scanpy.tl.draw_graph() function. A 200-node tree was fitted to the diffusion space using the simplePPT approach[94], with the parameter ppt_lambda set to 0.02. Pseudotime was subsequently calculated, with node 155 set as the root.

Bifurcation analysis

To identify genes with significant changes along the tree, an A cut parameter value of 0.25 was used. Significant genes were fitted using a generated additive model[95] to obtain smoothed trends. Subsequently, differential expression analysis was conducted to identify genes showing the most significant amplitude differences across branches. Each significant gene was tested for branch-specific differential gene expression, with a focus on upregulation from progenitor to terminal states. DEGs were assigned to two post-bifurcation branches, with an FDR threshold of < 0.05 and minimum expression difference cutoff of 0.05.

Gene regulatory network

Using a pseudobulk approach, the gene expression matrix was initially pseudobulked using the decoupler.get_pseudobulk() function. Subsequently, low-quality samples were filtered using the decoupler.filter_by expr_function() in the decoupleR Python package (v1.8.0)[41,96]. Differential expression analysis was performed between the $CD56^{dim}$ (canonical) and $CD56^{dim}$ (adaptive) subsets using the pydeseq2.dds.DeseqDataset() class in PyDESeq2 (0.4.11)[97]. TF enrichment scores were determined using a univariate linear model with CollecTRI to identify transcriptional regulatory interactions[98]. Regulon scores were calculated using the decoupler.run_

aucell() function, a wrapper for AUCell[99]. The top 20 TFs by enrichment score, along with their respective regulons registered in CollecTRI, were visualized using Cytoscape (v3.10.3)[100].

Data availability

The raw scRNA-seq data from recovered patients with severe COVID-19 and healthy individuals who received the SARS-COV-2 mRNA vaccine are deposited in the BioProject database under accession number PRJNA1152718 (https://dataview.ncbi.nlm.nih.gov/object/PRJNA1152718), where they are publicly accessible.

Received: 28 January 2025; Accepted: 10 July 2025
Published online: 28 October 2025

References

1. Lanier, L. L. Five decades of natural killer cell discovery. *J. Exp. Med.* **221**, 452. https://doi.org/10.1084/jem.20231222 (2024).
2. Nagler, A., Lanier, L. L., Cwirla, S. & Phillips, J. H. Comparative studies of human FcRIII-positive and negative natural killer cells. *J. Immunol.* **143**, 3183–3191 (1989).
3. Cooper, M. A., Fehniger, T. A. & Caligiuri, M. A. The biology of human natural killer-cell subsets. *Trends Immunol.* **22**, 633–640. https://doi.org/10.1016/s1471-4906(01)02060-9 (2001).
4. Crinier, A. et al. Single-cell profiling reveals the trajectories of natural killer cell differentiation in bone marrow and a stress signature induced by acute myeloid leukemia. *Cell Mol. Immunol.* **18**, 1290–1304. https://doi.org/10.1038/s41423-020-00574-8 (2021).
5. Ruckert, T., Lareau, C. A., Mashreghi, M. F., Ludwig, L. S. & Romagnani, C. Clonal expansion and epigenetic inheritance of long-lasting NK cell memory. *Nat. Immunol.* **23**, 1551–1563. https://doi.org/10.1038/s41590-022-01327-7 (2022).
6. Rebuffet, L. et al. High-dimensional single-cell analysis of human natural killer cell heterogeneity. *Nat. Immunol.* **25**, 1474–1488. https://doi.org/10.1038/s41590-024-01883-0 (2024).
7. Sun, J. C., Beilke, J. N. & Lanier, L. L. Adaptive immune features of natural killer cells. *Nature* **457**, 557–561. https://doi.org/10.1038/nature07665 (2009).
8. Freud, A. G., Mundy-Bosse, B. L., Yu, J. & Caligiuri, M. A. The broad spectrum of human natural killer cell diversity. *Immunity* **47**, 820–833. https://doi.org/10.1016/j.immuni.2017.10.008 (2017).
9. Haroun-Izquierdo, A. et al. Adaptive single-KIR(+)NKG2C(+) NK cells expanded from select superdonors show potent missing-self reactivity and efficiently control HLA-mismatched acute myeloid leukemia. *J. Immunother. Cancer* **10**, 412. https://doi.org/10.1136/jitc-2022-005577 (2022).
10. Barnes, S. A., Trew, I., de Jong, E. & Foley, B. Making a killer: selecting the optimal natural killer cells for improved immunotherapies. *Front. Immunol.* **12**, 765705. https://doi.org/10.3389/fimmu.2021.765705 (2021).
11. Costa-Garcia, M. et al. Human cytomegalovirus antigen presentation by HLA-DR+ NKG2C+ adaptive NK cells specifically activates polyfunctional effector memory CD4+ T lymphocytes. *Front. Immunol.* **10**, 687. https://doi.org/10.3389/fimmu.2019.00687 (2019).
12. Cooper, M. A. et al. Cytokine-induced memory-like natural killer cells. *Proc. Natl. Acad. Sci. U. S. A.* **106**, 1915–1919. https://doi.org/10.1073/pnas.0813192106 (2009).
13. Hammer, Q. et al. Peptide-specific recognition of human cytomegalovirus strains controls adaptive natural killer cells. *Nat. Immunol.* **19**, 453–463. https://doi.org/10.1038/s41590-018-0082-6 (2018).
14. Guan, W. J. et al. Clinical characteristics of coronavirus disease 2019 in China. *N. Engl. J. Med.* **382**, 1708–1720. https://doi.org/10.1056/NEJMoa2002032 (2020).
15. Huang, C. et al. Clinical features of patients infected with 2019 novel coronavirus in Wuhan, China. *Lancet* **395**, 497–506. https://doi.org/10.1016/S0140-6736(20)30183-5 (2020).
16. Georg, P. et al. Complement activation induces excessive T cell cytotoxicity in severe COVID-19. *Cell* **185**, 493–512. https://doi.org/10.1016/j.cell.2021.12.040 (2022).
17. Lee, M. J. & Blish, C. A. Defining the role of natural killer cells in COVID-19. *Nat. Immunol.* **24**, 1628–1638. https://doi.org/10.1038/s41590-023-01560-8 (2023).
18. Zafarani, A. et al. Natural killer cells in COVID-19: from infection, to vaccination and therapy. *Future Virol.* https://doi.org/10.2217/fvl-2022-0040 (2023).
19. Kramer, B. et al. Early IFN-alpha signatures and persistent dysfunction are distinguishing features of NK cells in severe COVID-19. *Immunity* **54**, 2650–2669. https://doi.org/10.1016/j.immuni.2021.09.002 (2021).
20. Witkowski, M. et al. Untimely TGFbeta responses in COVID-19 limit antiviral functions of NK cells. *Nature* **600**, 295–301. https://doi.org/10.1038/s41586-021-04142-6 (2021).
21. Cox, A. et al. Targeting natural killer cells to enhance vaccine responses. *Trends Pharmacol. Sci.* **42**, 789–801. https://doi.org/10.1016/j.tips.2021.06.004 (2021).
22. Cuapio, A. et al. NK cell frequencies, function and correlates to vaccine outcome in BNT162b2 mRNA anti-SARS-CoV-2 vaccinated healthy and immunocompromised individuals. *Mol. Med.* **28**, 20. https://doi.org/10.1186/s10020-022-00443-2 (2022).
23. Yamaguchi, Y. et al. Consecutive BNT162b2 mRNA vaccination induces short-term epigenetic memory in innate immune cells. *JCI Insight* **7**, 45. https://doi.org/10.1172/jci.insight.163347 (2022).
24. Dann, E., Henderson, N. C., Teichmann, S. A., Morgan, M. D. & Marioni, J. C. Differential abundance testing on single-cell data using k-nearest neighbor graphs. *Nat. Biotechnol.* **40**, 245–253. https://doi.org/10.1038/s41587-021-01033-z (2022).
25. Bjorkstrom, N. K. et al. Expression patterns of NKG2A, KIR, and CD57 define a process of CD56dim NK-cell differentiation uncoupled from NK-cell education. *Blood* **116**, 3853–3864. https://doi.org/10.1182/blood-2010-04-281675 (2010).
26. Vanherberghen, B. et al. Classification of human natural killer cells based on migration behavior and cytotoxic response. *Blood* **121**, 1326–1334. https://doi.org/10.1182/blood-2012-06-439851 (2013).
27. Wu, Z. et al. Human cytomegalovirus infection promotes expansion of a functionally superior cytoplasmic CD3(+) NK cell subset with a Bcl11b-regulated T cell signature. *J. Immunol.* **207**, 2534–2544. https://doi.org/10.4049/jimmunol.2001319 (2021).
28. Lanier, L. L. Natural killer cell receptor signaling. *Curr. Opin. Immunol.* **15**, 308–314. https://doi.org/10.1016/s0952-7915(03)00039-6 (2003).
29. Hesslein, D. G., Takaki, R., Hermiston, M. L., Weiss, A. & Lanier, L. L. Dysregulation of signaling pathways in CD45-deficient NK cells leads to differentially regulated cytotoxicity and cytokine production. *Proc. Natl. Acad. Sci. U. S. A.* **103**, 7012–7017. https://doi.org/10.1073/pnas.0601851103 (2006).
30. Adams, N. M., Grassmann, S. & Sun, J. C. Clonal expansion of innate and adaptive lymphocytes. *Nat. Rev. Immunol.* **20**, 694–707. https://doi.org/10.1038/s41577-020-0307-4 (2020).
31. Pfefferle, A. et al. Intra-lineage plasticity and functional reprogramming maintain natural killer cell repertoire diversity. *Cell Rep.* **29**, 2284–2294. https://doi.org/10.1016/j.celrep.2019.10.058 (2019).
32. Kwok, A. W. C. et al. MQuad enables clonal substructure discovery using single cell mitochondrial variants. *Nat. Commun.* **13**, 1205. https://doi.org/10.1038/s41467-022-28845-0 (2022).

33. Faure, L., Soldatov, R., Kharchenko, P. V. & Adameyko, I. scFates: a scalable python package for advanced pseudotime and bifurcation analysis from single-cell data. *Bioinformatics* **39**, 452. https://doi.org/10.1093/bioinformatics/btac746 (2023).
34. Liu, W. et al. FcRgamma gene editing reprograms conventional NK cells to display key features of adaptive human NK cells. *iScience* **23**, 101709. https://doi.org/10.1016/j.isci.2020.101709 (2020).
35. Vosshenrich, C. A. & Di Santo, J. P. Developmental programming of natural killer and innate lymphoid cells. *Curr. Opin. Immunol.* **25**, 130–138. https://doi.org/10.1016/j.coi.2013.02.002 (2013).
36. Mao, A. P., Ishizuka, I. E., Kasal, D. N., Mandal, M. & Bendelac, A. Publisher Correction: A shared Runx1-bound Zbtb16 enhancer directs innate and innate-like lymphoid lineage development. *Nat. Commun.* **8**, 1933. https://doi.org/10.1038/s41467-017-01780-1 (2017).
37. Nabekura, T. et al. Themis2 regulates natural killer cell memory function and formation. *Nat. Commun.* **14**, 7200. https://doi.org/10.1038/s41467-023-42578-8 (2023).
38. Jaeger, N. et al. Diversity of group 1 innate lymphoid cells in human tissues. *Nat. Immunol.* **25**, 1460–1473. https://doi.org/10.1038/s41590-024-01885-y (2024).
39. Cichocki, F. et al. ARID5B regulates metabolic programming in human adaptive NK cells. *J. Exp. Med.* **215**, 2379–2395. https://doi.org/10.1084/jem.20172168 (2018).
40. Kim, D. K. et al. Human NKG2F is expressed and can associate with DAP12. *Mol. Immunol.* **41**, 53–62. https://doi.org/10.1016/j.molimm.2004.01.004 (2004).
41. Badia, I. M. P. et al. decoupleR: ensemble of computational methods to infer biological activities from omics data. *Bioinform. Adv.* **2**, vbac016. https://doi.org/10.1093/bioadv/vbac016 (2022).
42. Rollins, D. A., Coppo, M. & Rogatsky, I. Minireview: nuclear receptor coregulators of the p160 family: insights into inflammation and metabolism. *Mol. Endocrinol.* **29**, 502–517. https://doi.org/10.1210/me.2015-1005 (2015).
43. Wong, P. et al. T-BET and EOMES sustain mature human NK cell identity and antitumor function. *J. Clin. Invest.* **133**, 452. https://doi.org/10.1172/JCI162530 (2023).
44. Li, J. H. et al. MEF2C regulates NK cell effector functions through control of lipid metabolism. *Nat. Immunol.* **25**, 778–789. https://doi.org/10.1038/s41590-024-01811-2 (2024).
45. Levy, C., Khaled, M. & Fisher, D. E. MITF: master regulator of melanocyte development and melanoma oncogene. *Trends Mol. Med.* **12**, 406–414. https://doi.org/10.1016/j.molmed.2006.07.008 (2006).
46. Reyahi, A. et al. Foxf2 is required for brain pericyte differentiation and development and maintenance of the blood-brain barrier. *Dev. Cell* **34**, 19–32. https://doi.org/10.1016/j.devcel.2015.05.008 (2015).
47. Masternak, K. et al. CIITA is a transcriptional coactivator that is recruited to MHC class II promoters by multiple synergistic interactions with an enhanceosome complex. *Genes Dev.* **14**, 1156–1166 (2000).
48. Beckers, A., Alten, L., Viebahn, C., Andre, P. & Gossler, A. The mouse homeobox gene Noto regulates node morphogenesis, notochordal ciliogenesis, and left right patterning. *Proc. Natl. Acad. Sci. U. S. A.* **104**, 15765–15770. https://doi.org/10.1073/pnas.0704344104 (2007).
49. Bailey, C. M. & Hendrix, M. J. IRF6 in development and disease: a mediator of quiescence and differentiation. *Cell Cycle* **7**, 1925–1930. https://doi.org/10.4161/cc.7.13.6221 (2008).
50. Fossum, S. L. et al. Ets homologous factor (EHF) has critical roles in epithelial dysfunction in airway disease. *J. Biol. Chem.* **292**, 10938–10949. https://doi.org/10.1074/jbc.M117.775304 (2017).
51. Maucourant, C. et al. Natural killer cell immunotypes related to COVID-19 disease severity. *Sci. Immunol.* **5**, 745. https://doi.org/10.1126/sciimmunol.abd6832 (2020).
52. Wilk, A. J. et al. Multi-omic profiling reveals widespread dysregulation of innate immunity and hematopoiesis in COVID-19. *J. Exp. Med.* **218**, 452. https://doi.org/10.1084/jem.20210582 (2021).
53. Malengier-Devlies, B. et al. Severe COVID-19 patients display hyper-activated NK cells and NK cell-platelet aggregates. *Front. Immunol.* **13**, 861251. https://doi.org/10.3389/fimmu.2022.861251 (2022).
54. Basilio-Queiros, D. & Mischak-Weissinger, E. Natural killer cells- from innate cells to the discovery of adaptability. *Front. Immunol.* **14**, 1172437. https://doi.org/10.3389/fimmu.2023.1172437 (2023).
55. Judge, S. J. et al. Minimal PD-1 expression in mouse and human NK cells under diverse conditions. *J. Clin. Invest.* **130**, 3051–3068. https://doi.org/10.1172/JCI133353 (2020).
56. Pesini, C. et al. PD-1 is expressed in cytotoxic granules of NK cells and rapidly mobilized to the cell membrane following recognition of tumor cells. *Oncoimmunology* **11**, 2096359. https://doi.org/10.1080/2162402X.2022.2096359 (2022).
57. Davis, Z. et al. Low-density PD-1 expression on resting human natural killer cells is functional and upregulated after transplantation. *Blood Adv.* **5**, 1069–1080. https://doi.org/10.1182/bloodadvances.2019001110 (2021).
58. Guma, M. et al. Imprint of human cytomegalovirus infection on the NK cell receptor repertoire. *Blood* **104**, 3664–3671. https://doi.org/10.1182/blood-2004-05-2058 (2004).
59. Fang, D. et al. Differential regulation of transcription factor T-bet induction during NK cell development and T helper-1 cell differentiation. *Immunity* **55**, 639–655. https://doi.org/10.1016/j.immuni.2022.03.005 (2022).
60. Schlums, H. et al. Cytomegalovirus infection drives adaptive epigenetic diversification of NK cells with altered signaling and effector function. *Immunity* **42**, 443–456. https://doi.org/10.1016/j.immuni.2015.02.008 (2015).
61. Marchal, C., Defossez, P. A. & Miotto, B. Context-dependent CpG methylation directs cell-specific binding of transcription factor ZBTB38. *Epigenetics* **17**, 2122–2143. https://doi.org/10.1080/15592294.2022.2111135 (2022).
62. Allan, D. S. J. et al. Expanded NK cells used for adoptive cell therapy maintain diverse clonality and contain long-lived memory-like NK cell populations. *Mol. Ther. Oncol.* **28**, 74–87. https://doi.org/10.1016/j.omto.2022.12.006 (2023).
63. Gatto, I. et al. Cytomegalovirus blood reactivation in COVID-19 critically ill patients: risk factors and impact on mortality. *Intensive Care Med.* **48**, 706–713. https://doi.org/10.1007/s00134-022-06716-y (2022).
64. Luyt, C. E. et al. Herpesviridae lung reactivation and infection in patients with severe COVID-19 or influenza virus pneumonia: a comparative study. *Ann. Intensive Care* **12**, 87. https://doi.org/10.1186/s13613-022-01062-0 (2022).
65. Hammer, Q. et al. SARS-CoV-2 Nsp13 encodes for an HLA-E-stabilizing peptide that abrogates inhibition of NKG2A-expressing NK cells. *Cell Rep.* **38**, 110503. https://doi.org/10.1016/j.celrep.2022.110503 (2022).
66. Hasan, M. Z. et al. SARS-CoV-2 infection induces adaptive NK cell responses by spike protein-mediated induction of HLA-E expression. *Emerg. Microbes Infect.* **13**, 2361019. https://doi.org/10.1080/22221751.2024.2361019 (2024).
67. Graydon, E. K. et al. Natural killer cells and BNT162b2 mRNA vaccine reactogenicity and durability. *Front. Immunol.* **14**, 1225025. https://doi.org/10.3389/fimmu.2023.1225025 (2023).
68. Tsang, H. W. et al. The central role of natural killer cells in mediating acute myocarditis after mRNA COVID-19 vaccination. *Med* **5**, 335–347. https://doi.org/10.1016/j.medj.2024.02.008 (2024).
69. Davis-Porada, J. et al. Maintenance and functional regulation of immune memory to COVID-19 vaccines in tissues. *Immunity* **57**, 2895–2913. https://doi.org/10.1016/j.immuni.2024.10.003 (2024).
70. Docherty, A. B. et al. Features of 20 133 UK patients in hospital with covid-19 using the ISARIC WHO Clinical Characterisation Protocol: prospective observational cohort study. *BMJ* **369**, m1985. https://doi.org/10.1136/bmj.m1985 (2020).
71. Vitale, C. et al. The corticosteroid-induced inhibitory effect on NK cell function reflects down-regulation and/or dysfunction of triggering receptors involved in natural cytotoxicity. *Eur. J. Immunol.* **34**, 3028–3038. https://doi.org/10.1002/eji.200425418 (2004).

72. Morgan, D. J. & Davis, D. M. Distinct effects of dexamethasone on human natural killer cell responses dependent on cytokines. *Front. Immunol.* **8**, 432. https://doi.org/10.3389/fimmu.2017.00432 (2017).
73. Plotz, F. B. et al. Mechanical ventilation alters the immune response in children without lung pathology. *Intens. Care Med.* **28**, 486–492. https://doi.org/10.1007/s00134-002-1216-7 (2002).
74. Raftery, M. J. F. et al. CAR NK cells: the future is now. *Annu. Rev. Cancer Biol.* **7**, 229–246. https://doi.org/10.1146/annurev-cancerbio-061521-082320 (2023).
75. Christodoulou, I. et al. Glycoprotein targeted CAR-NK cells for the treatment of SARS-CoV-2 infection. *Front. Immunol.* **12**, 763460. https://doi.org/10.3389/fimmu.2021.763460 (2021).
76. Lu, T. et al. Off-the-shelf CAR natural killer cells secreting IL-15 target spike in treating COVID-19. *Nat. Commun.* **13**, 2576. https://doi.org/10.1038/s41467-022-30216-8 (2022).
77. Zheng, G. X. et al. Massively parallel digital transcriptional profiling of single cells. *Nat. Commun.* **8**, 14049. https://doi.org/10.1038/ncomms14049 (2017).
78. Wolf, F. A., Angerer, P. & Theis, F. J. SCANPY: large-scale single-cell gene expression data analysis. *Genome Biol.* **19**, 15. https://doi.org/10.1186/s13059-017-1382-0 (2018).
79. Wolock, S. L., Lopez, R. & Klein, A. M. Scrublet: computational identification of cell doublets in single-cell transcriptomic data. *Cell Syst.* **8**, 281–291. https://doi.org/10.1016/j.cels.2018.11.005 (2019).
80. Korsunsky, I. et al. Fast, sensitive and accurate integration of single-cell data with Harmony. *Nat. Methods* **16**, 1289–1296. https://doi.org/10.1038/s41592-019-0619-0 (2019).
81. McInnes, L. H. J., Melville, J. UMAP: uniform manifold approximation and projection for dimension reduction. *arXiv*, https://doi.org/10.48550/arXiv.1802.03426 (2020).
82. Yang, C. et al. Heterogeneity of human bone marrow and blood natural killer cells defined by single-cell transcriptome. *Nat. Commun.* **10**, 3931. https://doi.org/10.1038/s41467-019-11947-7 (2019).
83. Traag, V. A., Waltman, L. & van Eck, N. J. From Louvain to Leiden: guaranteeing well-connected communities. *Sci. Rep.* **9**, 5233. https://doi.org/10.1038/s41598-019-41695-z (2019).
84. Satija, R., Farrell, J. A., Gennert, D., Schier, A. F. & Regev, A. Spatial reconstruction of single-cell gene expression data. *Nat. Biotechnol.* **33**, 495–502. https://doi.org/10.1038/nbt.3192 (2015).
85. Heumos, L. J. et al. Pertpy: an end-to-end framework for perturbation analysis. *BioRxiv.* https://doi.org/10.1101/2024.08.04.606516v1 (2024).
86. Fang, Z., Liu, X. & Peltz, G. GSEApy: a comprehensive package for performing gene set enrichment analysis in Python. *Bioinformatics* **39**, 452. https://doi.org/10.1093/bioinformatics/btac757 (2023).
87. Chen, E. Y. et al. Enrichr: interactive and collaborative HTML5 gene list enrichment analysis tool. *BMC Bioinform.* **14**, 128. https://doi.org/10.1186/1471-2105-14-128 (2013).
88. Kuleshov, M. V. et al. Enrichr: a comprehensive gene set enrichment analysis web server 2016 update. *Nucleic Acids Res.* **44**, W90-97. https://doi.org/10.1093/nar/gkw377 (2016).
89. Xie, Z. et al. Gene set knowledge discovery with enrichr. *Curr. Protoc.* **1**, e90. https://doi.org/10.1002/cpz1.90 (2021).
90. Huang, X. & Huang, Y. Cellsnp-lite: an efficient tool for genotyping single cells. *Bioinformatics* **37**, 4569–4571. https://doi.org/10.1093/bioinformatics/btab358 (2021).
91. Sturm, G. et al. Scirpy: a Scanpy extension for analyzing single-cell T-cell receptor-sequencing data. *Bioinformatics* **36**, 4817–4818. https://doi.org/10.1093/bioinformatics/btaa611 (2020).
92. Setty, M. et al. Characterization of cell fate probabilities in single-cell data with Palantir. *Nat. Biotechnol.* **37**, 451–460. https://doi.org/10.1038/s41587-019-0068-4 (2019).
93. Jacomy, M., Venturini, T., Heymann, S. & Bastian, M. ForceAtlas2, a continuous graph layout algorithm for handy network visualization designed for the Gephi software. *PLoS ONE* **9**, e98679. https://doi.org/10.1371/journal.pone.0098679 (2014).
94. Mao, Q. Y., L.; Wangz, L.; Goodisonx, S.; Sun, Y. SimplePPT: a simple principal tree algorithm. In *Proceedings of the 2015 SIAM International Conference on Data Mining (SDM) 792–800 (Society for Industrial and Applied Mathematics, 2015).* https://doi.org/10.1137/1.9781611974010.89 (2015).
95. Wood, S. N. *Generalized Additive Models: An Introduction with R, Second Edition* (CRC, 2017).
96. Squair, J. W. et al. Confronting false discoveries in single-cell differential expression. *Nat. Commun.* **12**, 5692. https://doi.org/10.1038/s41467-021-25960-2 (2021).
97. Muzellec, B., Telenczuk, M., Cabeli, V. & Andreux, M. PyDESeq2: a python package for bulk RNA-seq differential expression analysis. *Bioinformatics* **39**, 145. https://doi.org/10.1093/bioinformatics/btad547 (2023).
98. Muller-Dott, S. et al. Expanding the coverage of regulons from high-confidence prior knowledge for accurate estimation of transcription factor activities. *Nucleic Acids Res.* **51**, 10934–10949. https://doi.org/10.1093/nar/gkad841 (2023).
99. Aibar, S. et al. SCENIC: single-cell regulatory network inference and clustering. *Nat. Methods* **14**, 1083–1086. https://doi.org/10.1038/nmeth.4463 (2017).
100. Shannon, P. et al. Cytoscape: a software environment for integrated models of biomolecular interaction networks. *Genome Res.* **13**, 2498–2504. https://doi.org/10.1101/gr.1239303 (2003).

Acknowledgements

We thank Fuminori Sugihara (iFReC) and the NGS Core Facility (RIMD) for their assistance in this study. We acknowledge the support provided to Yosuke Kishi by the Osaka University Medical Doctor Scientist Training Program during the course of this research. Illustrations were created using BioRender (https://BioRender.com).

Author contributions

YK: Investigation, validation, visualization, and writing——original draft and editing. YL: Investigation, validation, visualization, and writing——original draft and editing. MI: Investigation; MY: Investigation; HM: Resources; validation; writing——review and editing. HO: Resources, writing——review and editing. SS: Conceptualization, writing——original draft and editing. DO: Project administration, funding acquisition, writing——review and editing.

Competing interests

The authors declare no competing interests.

Additional information

Supplementary Information The online version contains supplementary material available at https://doi.org/10.1038/s41598-025-11575-w.

Correspondence and requests for materials should be addressed to S.S. or D.O.